Local surface aeration at hydraulic structures   2

HELMUT KOBUS & HANS-PETER KOSCHITZKY
Institut für Wasserbau, Universität Stuttgart, Germany

2.1 INTRODUCTION

In open channel flows, local surface aeration processes occur mainly at weirs and drop structures and in hydraulic jumps. Air entrainment in the wakes of bluff bodies is observed only in high speed flows.

In water pollution abatement, the natural gas exchange at the free surface is sometimes not sufficient to balance the oxygen consumption due to pollutants. In such cases, local aeration is needed in order to increase the oxygen transfer into the water body. In this context, hydraulic structures leading to local surface aeration provide the increased oxygen transfer by way of the entrained air bubbles. Thus the air-entrainment and oxygen-transfer characteristics have become an important design criterion for many hydraulic structures. Contrary to the structural design considerations, which would seek to avoid air entrainment, water quality considerations are geared towards increasing the air entrainment rates.

Local surface aeration processes are a complex phenomena which depend sensitively upon many parameters. The boundary geometry and the absolute scales of geometry and flow rates are extremely important. Therefore, no generally applicable design criteria can be formulated. Each of the flow configurations described in Chapter 1 and each of the various limitations of the entraining process have to be studied in detail.

The following material is a summary of the available information about local air entrainment and oxygen transfer, and it is intended to serve as an orientation for preliminary design considerations. Limited results can be presented for a small number of flow geometries. These results can only be used for similar geometries; the flow configurations must really be comparable. Application of these results to other flow configurations could lead to erroneous estimates.

The majority of results presented here stems from laboratory investigations at small scales. These data can only be safely applied within the range of scales and discharges in which they have been obtained. This range is therefore quoted for all

empirical relationships. Extrapolations beyond this range are risky because of possible scale effects involed (Kobus, 1984).

Because of the absence of generally applicable standard design criteria, the following chapter can only identify the major effects involved in local aeration, give the available data for standard geometries, and discuss the similarity considerations for hydraulic model studies.

2.2 PARAMETERS GOVERNING LOCAL AERATION

In most cases of local aeration, air entrainment takes place at a discontinuity of the free surface at which substantial velocity differences are encountered. In a hydraulic jump, for instance, the air is entrained exclusively at the toe of the surface roller. Jets impinging on and penetrating into a stagnant water body entrain air around the circumference of the jet intersection with the free water surface. The essential local parameters governing the entrainment process are
  – the velocity v_e (or velocity difference) at the line of air entrainment;
  – the length (width) of the intersection line, at which air is entrained;
  – density ρ_w and gravity g;
  – the character (smoothness) of the water surface at the line of air entrainment.
This is characterized by the intensity and scale of the turbulence of the approach flow and possibly also by the air content of the approach flow.

If the governing local parameters are common to all configurations, one may distinguish
  – The *outer problem:* How do these local characteristics depend upon the system parameters of the structure?
  – The *inner problem:* How does the air entrainment depend upon the local characteristics?

A crucial feature of the *inner problem* is the absence of a physically meaningful geometric boundary reference length for the air entrainment process. The significant length terms are the turbulent eddy size and the air pocket size, and both are dependent variables governed by the fluid properties and the flow. That is, they are not prescribed by the boundary configuration. The water depth or jet width (as geometric boundary length) is in most cases irrelevant and only important at small values (order of magnitude 0.01 m).

The process of air entrainment can be visualized as air pockets first being trapped between roller or water surface and inflow, and then carried downstream by the mean flow. The size and frequency of formation of such pockets can be expected to depend upon the differential velocity between the receiving water volume and the inflow, or – since the velocity of the receiving water volume is zero in the mean – upon the velocity of the inflow alone. This velocity governs the turbulent shear stress generated in the shear layer at the entrainment location. Obviously, the boundary scale – for instance, the water depth or jet width – will in

most cases have no influence upon the entrainment process unless it is small enough to be of the order of the enclosed air pockets. This fact can be used to deduce some information about the inception and entrainment limits.

In Chapter 1, the distinction was made between plunging jets and surface rollers, the former being predominantly vertical and the latter predominantly horizontal.

2.3 INCEPTION LIMIT

The inception of air entrainment is governed by the condition that the free surface is penetrated and interrupted by the impinging flow. Air entrainment will commence when inertial and gravity forces override the resisting forces due to viscosity and surface tension. Therefore, the *critical* velocity v_c for onset of aeration will depend, for given approach flow conditions, on the following fluid properties:

$$f(v_c; \rho_w; g; \mu_w.\sigma_{wa}) = 0 \tag{2.1}$$

These can be grouped into two dimensionless parameters:

$$f\left(\frac{v_c^3}{g\mu_w/\rho_w} ; \frac{g\mu_w^4}{\rho_w\sigma_{wa}^3}\right) = f\left(\frac{v_c^3}{gv_w} ; Z\right) = 0 \tag{2.2}$$

Equation 2.2 indicates that the nondimensional critical velocity will depend upon the magnitude of the liquid parameter Z, and if Z is kept constant (constant water quality and temperature), the inception limit is characterized by

$$\frac{v_c^3}{g\mu_w/\rho_w} = \text{const} \approx (0.5 \text{ to } 1) \times 10^5 \tag{2.3}$$

The figure given is a rough estimate taken from experimental evidence for plunging water jets, and it indicates that air entrainment commences at velocities of 0.8 to 1 m/s.

Equation 2.3 indicates further that the inception limit corresponds neither to a constant Reynolds number nor to a constant Froude number.

If the approach flow is turbulent, two additional parameters must be introduced to characterize the intensity and the scale of the turbulent fluctuations. If v_t denotes the RMS of the velocity fluctuations and l_t is a turbulence length scale, then one arrives by dimensional analysis at

$$\frac{v_c^3}{g\mu_w/\rho_w} = f\left(\frac{v_t}{\mu_w^3 g/\sigma_{aw}^2\rho_w} ; \frac{l_t}{\sigma_{aw}^2/\mu_w^2 g} ; (Z)\right) \tag{2.4}$$

where ($\sigma_{wa}^2/\mu_w^2 g$) is a length based on the fluid properties and gravity.

A physical concept of the plunge point inception has been outlined by Thomas, (1982). It relates air entrainment to the fact that the plunge pool water is unable to follow undulations of the jet surface and hence small air pockets are formed. Surface undulations in turn are produced by the turbulence in the jet as indicated by Equation 2.4.

The experimental results for plunging jets obtained by Ervine et al. (1980) indicate that the critical velocity depends strongly upon the turbulent velocity fluctuations v_t, whereas the jet diameter and hence the scale l_t of the large eddies in the approach flow are insignificant. For given fluid properties (Z = const) the critical velocity v_c will therefore depend upon the relative turbulence (v_t/v_w) or (v_t/v_c). Ervine's results for jet diameters of 6, 9, 14 and 25 mm are plotted in Figure 2.1. For larger turbulence intensities v_c is almost constant in the range of 0.8 to 1 m/s. Ervine suggests further that for an impinging rectangular water jet the critical velocity is also in the same range. Observations by Casteleyn & Kolkman (1978) on siphons also indicate critical velocities of approximately 0.8 m/s.

The preceding discussion does not include the case of entrainment at a hydraulic jump. In addition to the mechanism described above, the unsteady flow in the surface roller above the entering jet greatly contributes to the entrainment by a jump. The turbulence intensity and scale in the surface roller increase with increasing Froude number of the approach flow. At Froude numbers slightly larger than one, unbroken surface waves without air are observed. According to Henderson (1971), the entrainment processes commence at Froude numbers larger than about 1.7.

Finally, for flows with a mean velocity parallel to the air-water surface as on a spillway, no impingement takes place. Thus, although Equation 2.4 still holds, the value of v_c must be expected to be much larger than the values given above. From considerations of the turbulent characteristics of high speed flows, Ervine (1985), came to the conclusion that free surface aeration occurs when the turbulent fluctuations in eddies close to the surface reach values of 0.25 to 0.30 m/s in small eddies of 0.001 to 0.01 m in size.

2.4   ENTRAINMENT LIMIT AND ENTRAINED AIR FLOW RATE

In the limiting case of fully turbulent flow (very high Reynolds numbers), the process of air entrainment finally becomes independent of viscosity, that is, the large-scale turbulence is governed by inertial reactions alone. In these cases the amount of air entrainment, expressed either as total flow rate or as flow rate per unit length of surface discontinuity, becomes

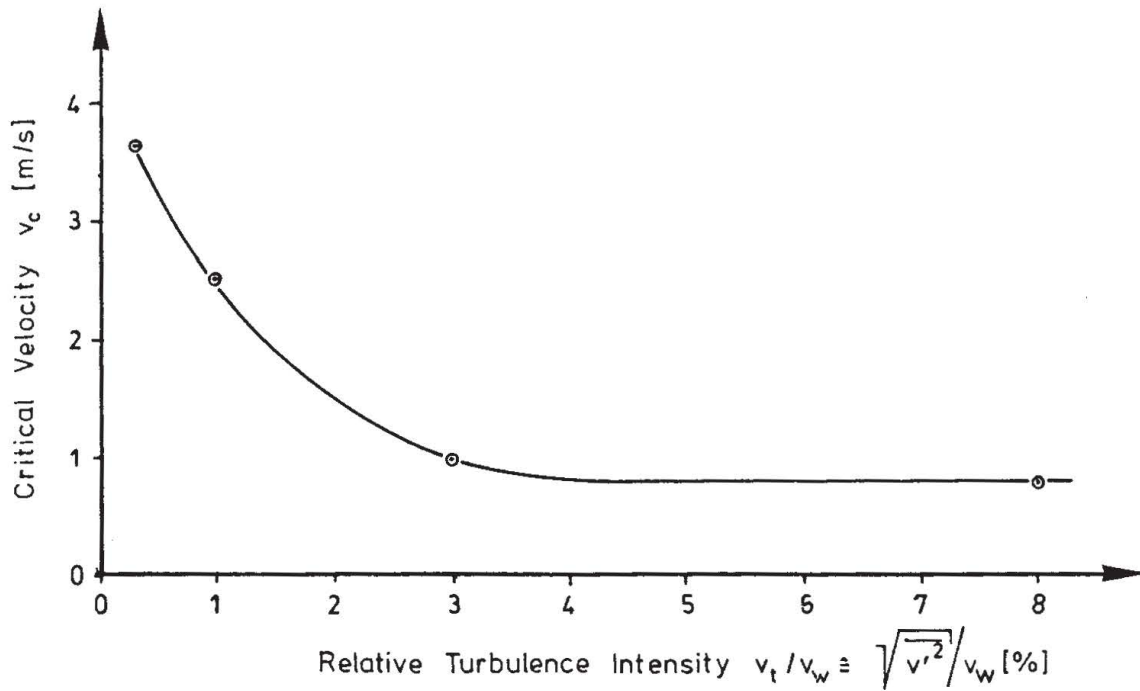$$Q_{ae}, q_{ae} = f_{1,2}(v_e; \rho_w; g) \tag{2.5}$$

Figure 2.1. The critical velocity for air entrainment in a plunging circular water jet (Ervine, 1980)

These terms lead to a single dimensionless parameter, which hence must necessarily attain a constant value:

$$\frac{Q_{ae}}{v_e^5/g^2} \; ; \frac{q_{ae}}{v_e^3/g} = \text{const}_{1,2} \tag{2.6}$$

This relationship, together with $(q_w = v_e.y_e)$ indicates

$$\frac{q_{ae}}{q_w} \equiv \beta_e = \text{const} \frac{v_e^2}{gy_e} = \text{const}\, Fr^2 = k_e Fr^2 \tag{2.7}$$

with k_e defined as an *entrainment coefficient*. In fully turbulent flow, k_e should in the limit attain a constant value for a given boundary geometry (and given approach flow). Hence the relative air entrainment should ultimately become directly proportional to the square of the local Froude number. However, the approach flow conditions (velocity profile, turbulence, air content) are seen to have a pronounced influence upon the entrainment process.

As an example of air entrainment governed by the limiting condition as given by Equation 2.7 is shown in Figures 2.2 and 2.3. Renner (1973) performed extensive experiments for the basic configuration of a jet impinging on an inclined wall. (This configuration is found e.g. in self-priming siphons with a deflector nose, in which the air entrainment observed here serves for evacuating the siphon

hood). In the impingement region, a surface roller forms and entrains air (Figure 2.2). The experimental results shown in Figure 2.3 clearly confirm Equation 2.7 over a wide range of Froude numbers; deviations from this relation are attributed to approaching the transport limit of the configuration.

In the general case, the viscosity μ_w and the turbulence characteristics Tu of the approach flow have to be added to the list of independent variables in Equation 2.5. This results in the following relation:

$$\beta_e = k_e(Re; Tu) \cdot Fr^2 \tag{2.8}$$

The factor Tu summarizes all relevant conditions of the approach flow which may
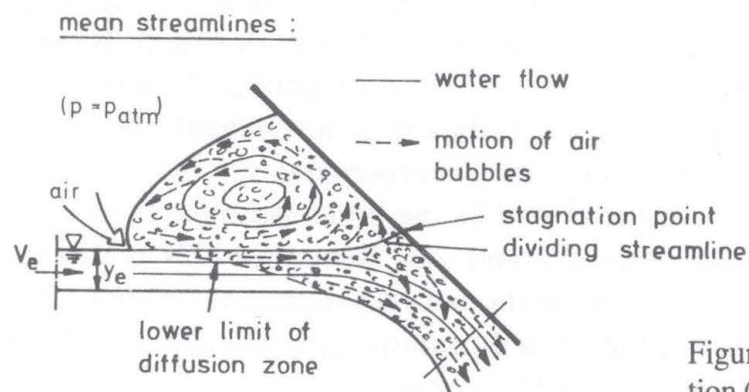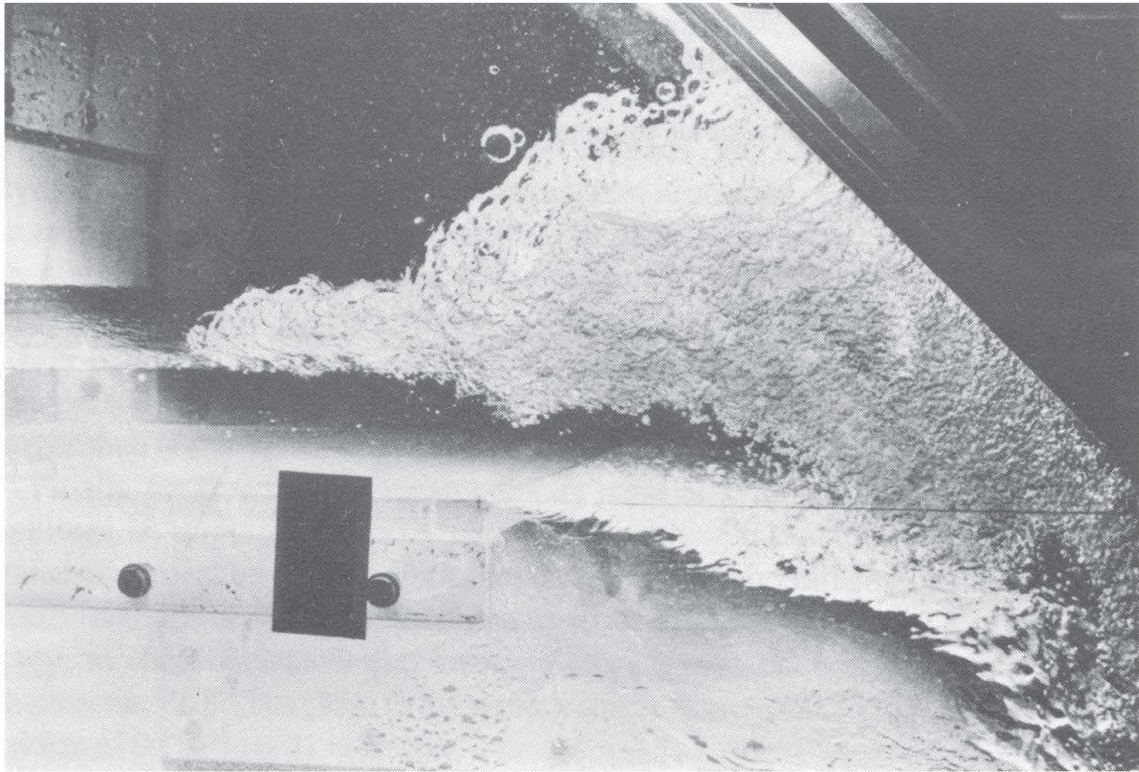

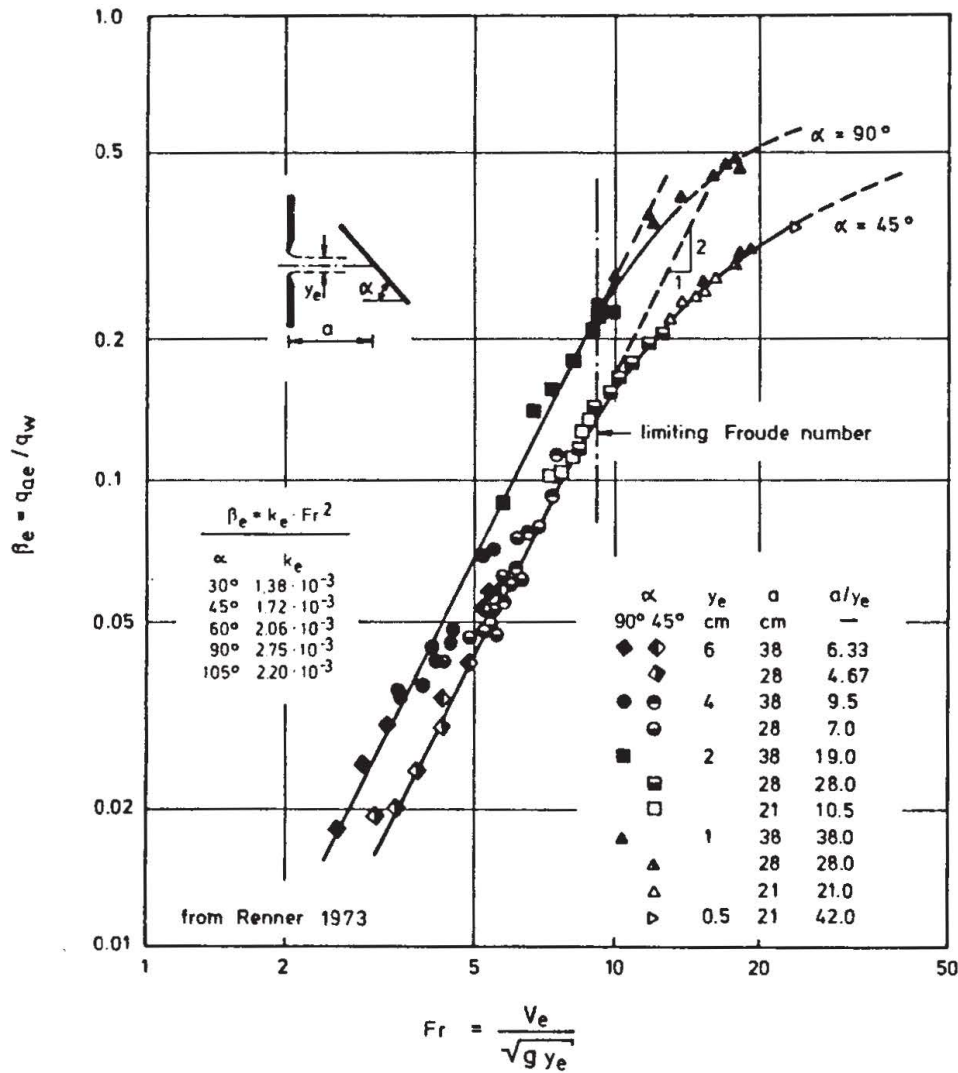Figure 2.2. Impinging jet configuration (Renner, 1973)

Figure 2.3. Air entrainment in impinging jets: correlation of experiments with Equation 2.7

be expected to have an influence on the mechanics of the entrainment process. These include the velocity distribution over the cross section, flow curvature, turbulence intensity and scale, and air content.

A different set of parameters which satisfies the condition that the air flux is zero when the velocity is less than the critical velocity, can be written as

$$\frac{Q_{a,e}}{(v-v_c)^5/g^2} = f(Re; Tu; Z) \tag{2.9}$$

For flows with large velocities

$$(v-v_c)/v \approx 1 \tag{2.10}$$

and in this case the relationship in Equation 2.9 reduces again to the relationship in Equation 2.8.

2.5 WEIRS AND DROP STRUCTURES

2.5.1 *Critical velocity*

Ervines's extensive investigations on the critical velocity for air entrainment in a plunging circular jet have led to the result shown in Figure 2.1. In technical applications the approach flow usually has a turbulence intensity of at least a few percent. Therefore, one obtains for practical purposes a critical velocity of

$$v_c \approx 0.80 \, \text{m/s} \tag{2.11}$$

This value should apply to any flow configuration of the plunging-jet-type, as long as the jet is still coherent at the point of impingement.

For jets with a great height of fall, air entrainment may commence in the free jet and the jet surface may disintegrate before it reaches the water surface. Jet disintegration will occur when the turbulent shear layers have spread from the outer edge to the centerline of the jet so that the inner core of the jet has decayed. This process has a strong effect on the air entrainment rate.

The distance L_o from the nozzle along the centerline of the nappe to the point of total disintegration depends upon the flow rate and the turbulence intensity of the jet flow. For circular jets, Ervine (1980) quotes the following relationship by Baron:

$$L_o/d_n = 537.6 \, We/Re^{5/8} \tag{2.12}$$

Ervine's experiments indicate the strong influence of the initial jet turbulence upon the distance L_o. In Figure 2.4 his results are shown in comparison to Equation 2.12. More recent experiments of Ervine (1985), at larger scales confirm the result that for typical jet turbulence intensities of 3 to 8%, the relative breakup length L_o/d_n is of the order of 50 to 100.

For plane nappes, Avery (1976) quotes an investigation of Horeni (1956) which is plotted in Figure 2.5. This relationship was visually confirmed by Avery. Outside the verified range, it may be useful for a first rough quess.

2.5.2 *Air entrainment rate*

For rectangular vertical drop shafts into which water is discharged in the form of a wall jet, Ervine (1980) has conducted numerous experiments over a wide range of conditions. The results are shown in Figure 2.6. His experiments for air entrainment on one side of the jet can be summarized by a mean correlation function for the air discharge per unit width of the form (Ervine, 1981).

$$\beta_e = q_{ae}/q_w = 0.0045 \, Fr^2 \, (1 - (v_c/v_w))^3 \qquad \text{with } v_c = 0.8 \, \text{m/s} \tag{2.13}$$
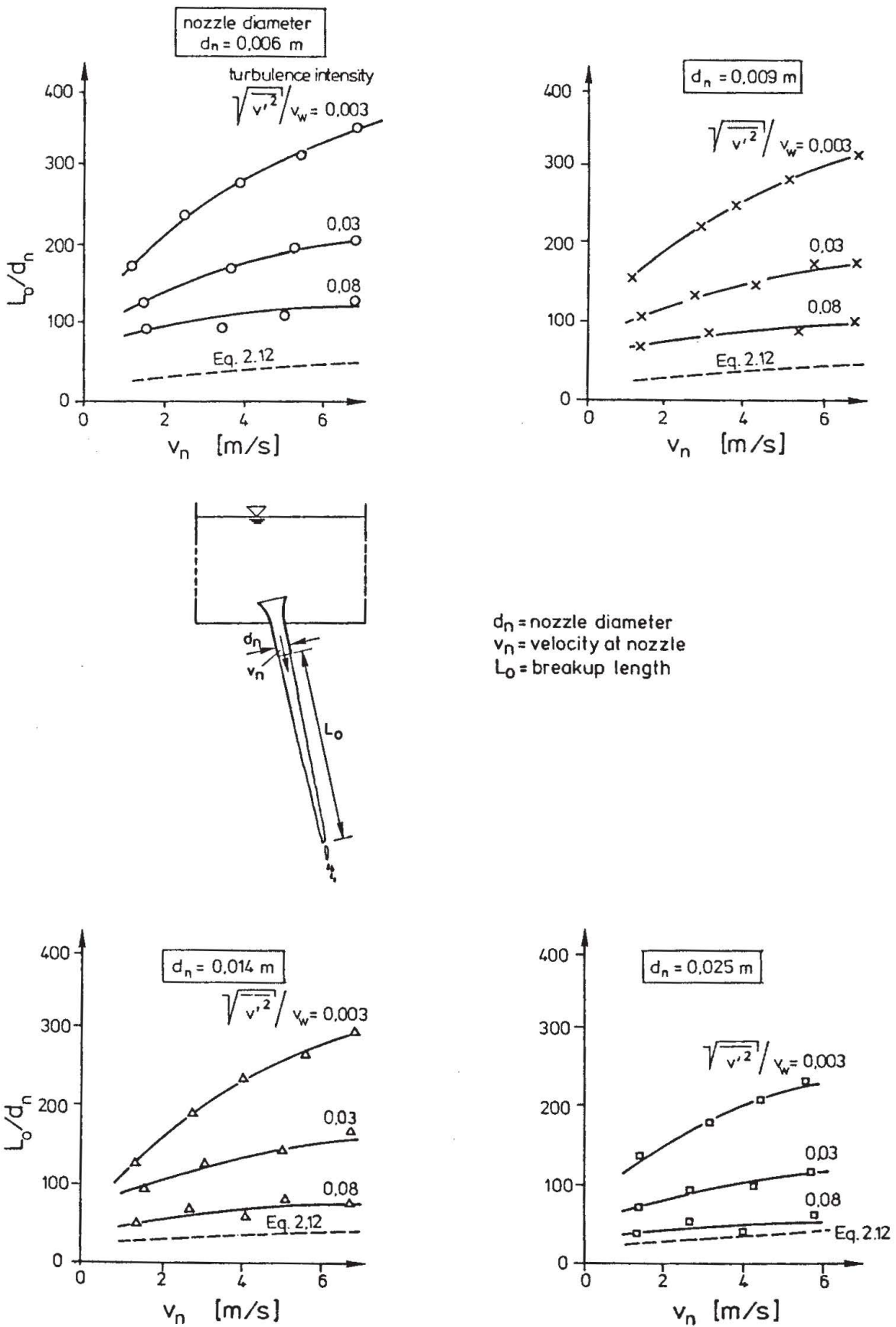
Figure 2.4. Relative break-up length L_o/d_n and jet velocity for circular nappes according to Ervine (1980)
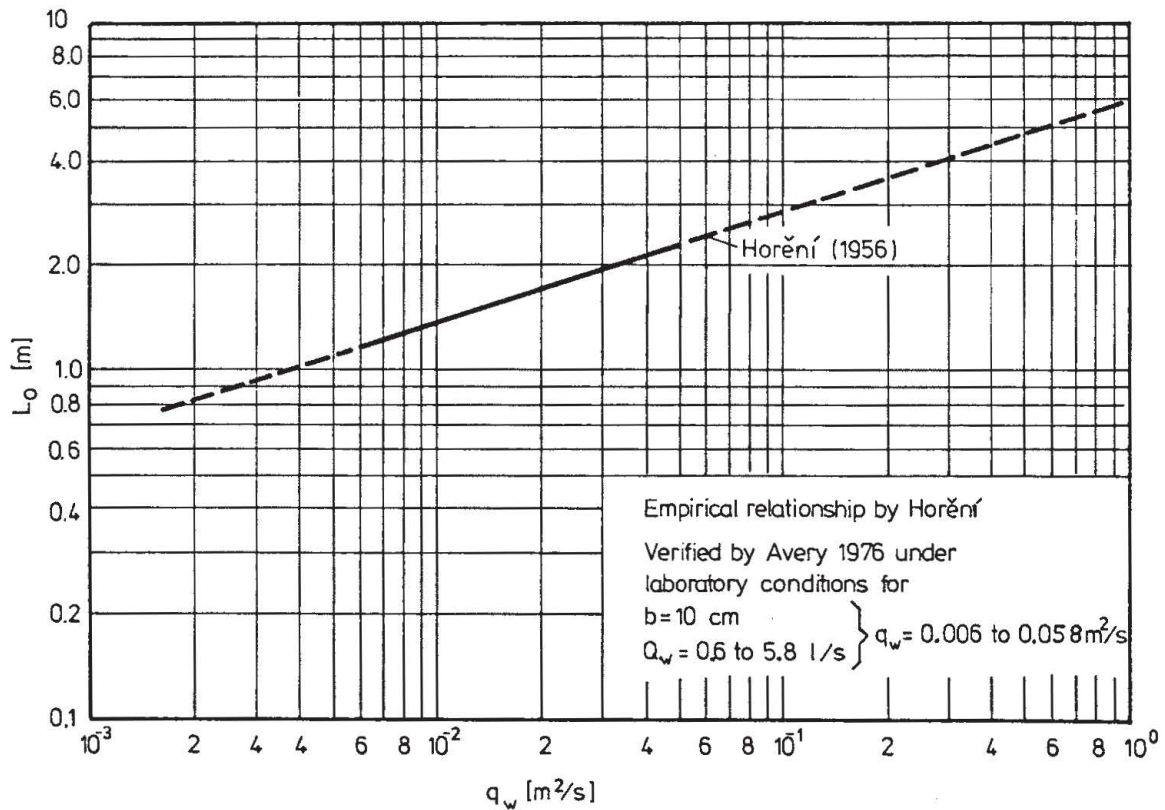
Figure 2.5. Jet break-up length L_o for plane nappes according to Avery (1976)

The bulk of the experimental data is within ± 20% of this relationship.

Equation 2.13 then provides adequate design information based on the following parameter range:

height of fall h: from 0.20 to 2.00 m
water velocities v at the point of impact: from 3.00 to 6.00 m/s

For the discharge over sharp-crested weirs, Equation 2.13 may provide an estimate for wide rectangular weirs without aeration (i.e. air is entrained only on one side). For aerated weirs, air is entrained also under the nappe, so that the length of entrainment is doubled and hence also the air entrainment rate may be expected to double.

For sharp crested weirs of limited width or of a shape deviating from the rectangular form, the air entrainment may be expected to vary with the shape of the jet at the impingement cross section. The deformation of a free falling nappe has been studied by Avery & Novak (1978). They define a Froude number on the basis of the jet discharge per unit jet perimeter
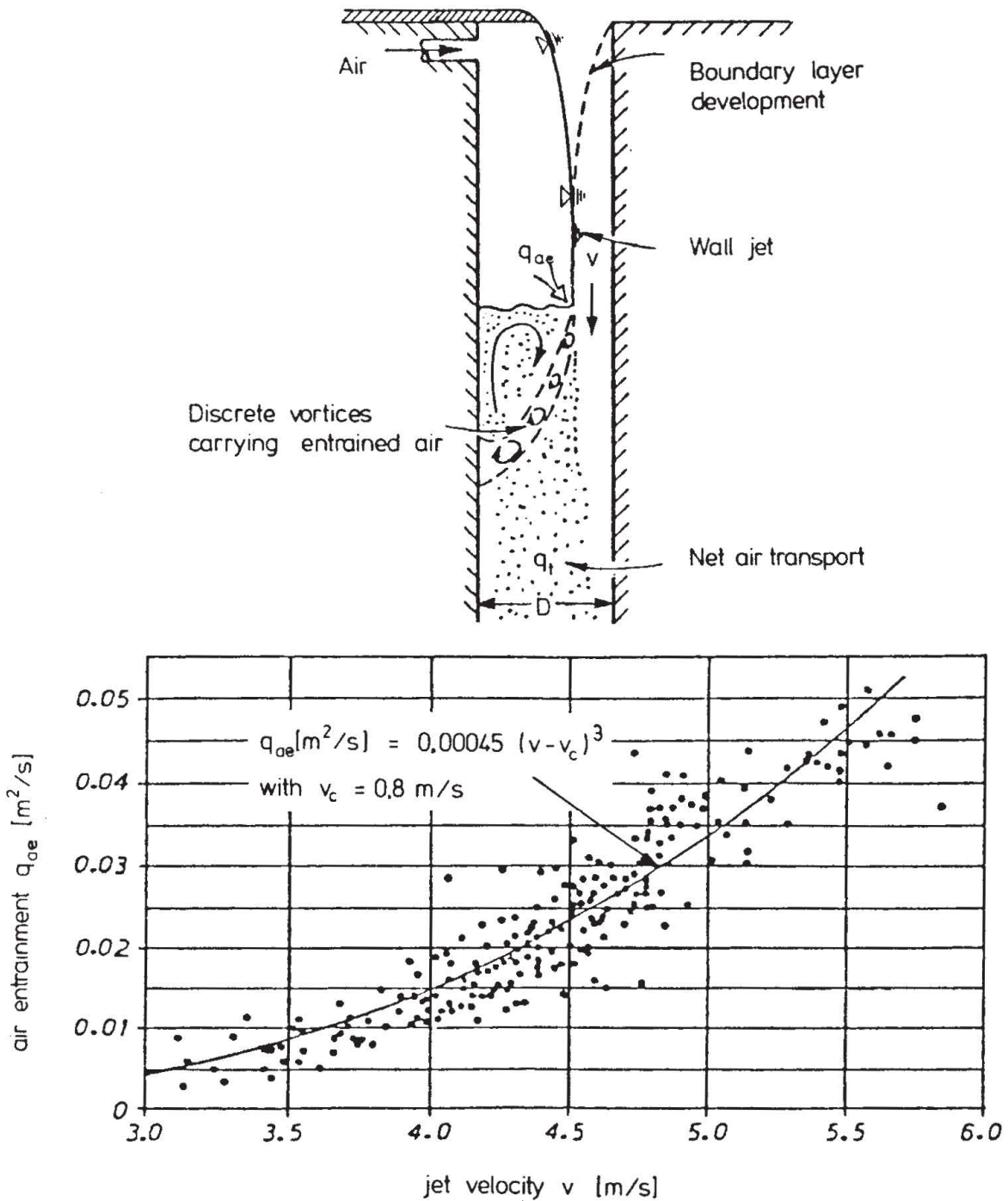
$$q_j = R \sqrt{2gh} \tag{2.14}$$

Figure 2.6. Ervine's experiments on air entrainment in plunging jets or drop shafts

where R is the hydraulic radius of the jet at impact (see Figure 2.7). With this, the jet Froude number is defined as

$$Fr_j = v/\sqrt{gd} = \left(\frac{\pi\sqrt{2gh^5}}{Q_w}\right)^{1/4} = \left(\frac{gh^3}{2q_j^2}\right)^{1/4} \tag{2.15}$$

Solid jets from a rectangular notch either converge fairly quickly to a circular cross section or diverge to flat rectangular shapes. The criterion for a jet to diverge is (Novak, 1980)

$$H/b > 1.288 : \text{divergent}$$
$$H/b < 1.288 : \text{convergent} \tag{2.16}$$

and the height h at which convergent jets become circular is given by the authors in dimensional form as

$$h \,|\text{m}| = 431 \, b^{0.36} \,|\text{m}| \, Q_w^{0.8} \,|\text{m}^3/\text{s}| \tag{2.17}$$

The air entrainment rate Q_{ae} can be assumed to be proportional to the total length l_p of jet surface intersection with the water surface, for wide rectangular jets, the intersection length l_p becomes twice the width B $(B/l_p \approx 1/2)$. For this case, Ervine & Elsawy (1975) give the following empirical relationship:

$$\beta_e = Q_{ae}/Q_w = 0.13(h/d)^{0.446} (1 - v_c/v) \tag{2.18}$$

from experiments covering the following range:

height of fall h: 0 to 2.0 m
water discharge Q_w: 0 to 0.1 m³/s
jet width B: 0 to 0.25 m
jet thickness d: 0 to 0.10 m
jet velocity v: 0 to 10 m/s

The minimum velocity to entrain air was found in these experiments to be approximately 1.1 m/s.

2.5.3 *Oxygen transfer characteristics*

For water quality purposes, local aeration processes are often welcome as means of increasing the oxygen content of the water. In these cases it is of interest to know the rate of mass transfer between air and water. This depends upon the concentration difference between air and water, upon the contact area, i.e. total surface area of the bubbles, and upon the surface renewal rate, i.e. turbulent mixing, contact times, and bubble trajectories. The process of reoxygenation can be considered in three consecutive steps:
   – mechanics of air entrainment;
   – mechanics of air transport away from the entrainment location, and
   – transfer of oxygen from the air bubbles into solution.
The first two steps depend upon hydrodynamics alone, whereas the third step
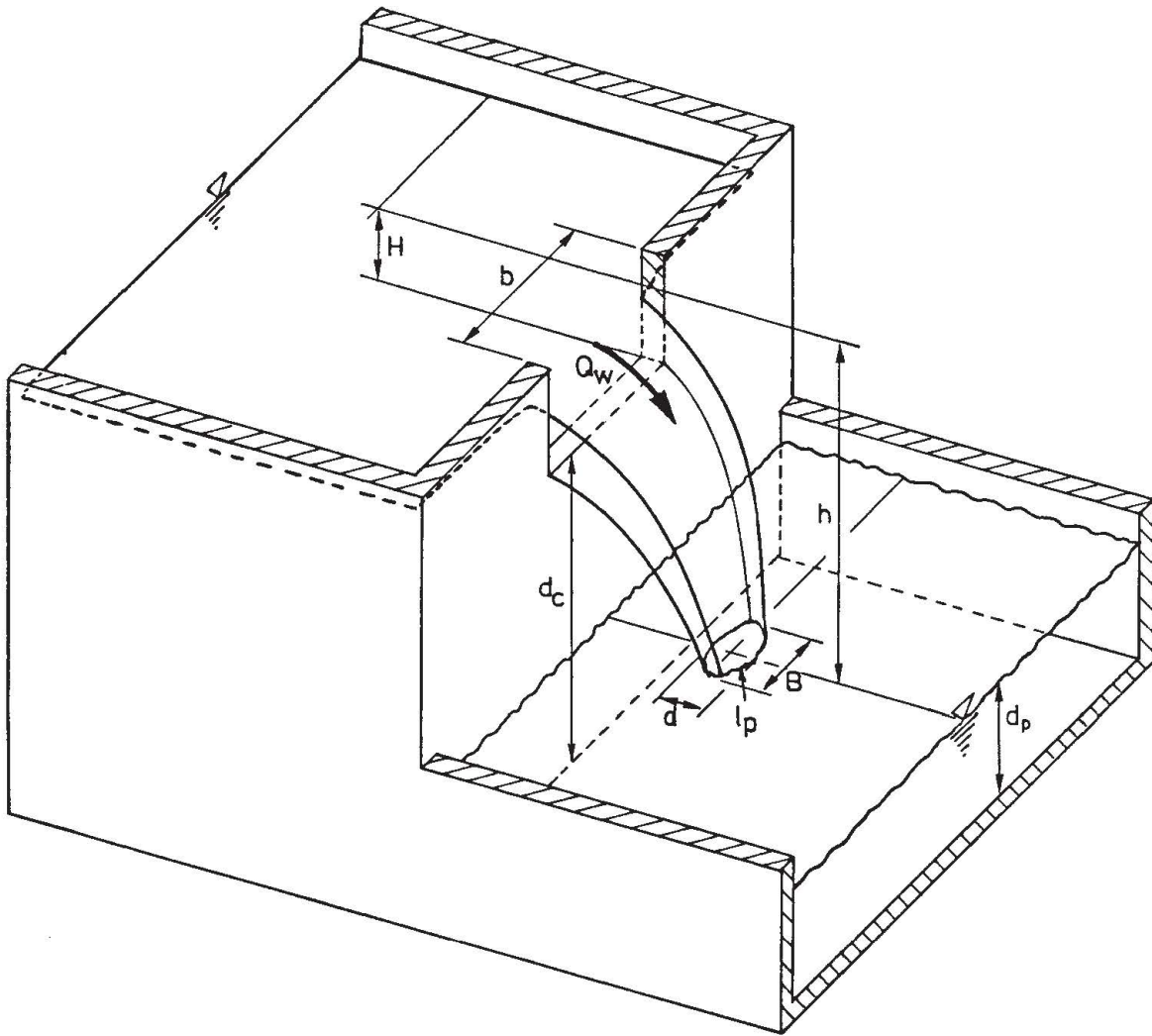
Figure 2.7. Definition sketch for plane nappes falling from a rectangular notch

represents the phase of the process which depends upon the properties of the water, such as temperature, initial dissolved oxygen content, salinity, and degree of water pollution.

The bubble trajectory or residence time will be governed by the same parameters as the air entrainment. However, the turbulence characteristics (scale and intensity) of the flow and hence the Reynolds number may have a marked influence upon the bubble transport.

The mass transfer is described by the increase in concentration in the water while passing the installation. For oxygenation, this is usually expressed in terms of the reoxygenation rate r in terms of oxygen concentration c as follows:

$$r \equiv \frac{C_{\text{Saturation}} - C_{\text{upstream}}}{C_{\text{Saturation}} - C_{\text{downstream}}} = \frac{\text{deficit upstream}}{\text{deficit downstream}} \geq 1 \qquad (2.19)$$

This coefficient r will again depend upon the same parameters as the air entrainment rate, as well as upon the additional parameters governing the mass transfer rate, such as water temperature, water quality and pressure conditions. Therefore, when comparing results on mass transfer from various investigations, one has to reduce the data to *standard conditions* with respect to these parameters.

In general, standard conditions are considered to be given for

- atmospheric pressure
- water temperature of 15°C
- good water quality.

Data reduction to this base is made by correction factors as follows. For temperature T, in °Celsius (from EPA, 1970):

$$f_T = \frac{(r-1)_T}{(r-1)_{15°C}} = \frac{1 + 0.046\,T}{1.69} \tag{2.20}$$

For water quality:

$$f_{wq} = \frac{(r-1)\ \text{given water quality}}{(r-1)\ \text{base water quality}} \tag{2.21}$$

with the following factors from WPR (1973) for laboratory data and from Gameson (1957) for field data:

	f_{wq1} (laboratory)	f_{wq2} (field)
Clean	1.00	–
Slightly polluted	0.89	1.00
Moderately polluted	0.56	0.81
Grossly polluted	0.36	0.69

As one example of a generalized data presentation on the basis described above, Markofsky & Kobus (1978) have developed a diagram for sharp crested aerated rectangular weirs discharging into a deep plunging pool. All available model and field data are plotted in Figure 2.8 and describe in a consistent fashion the relation between observations at various scales. This figure clearly indicates the effects of scale. However, the nomogram is not intended for prediction of weir reoxygenation at a given location, and should not be used for predictions without proper caution and consideration of the restrictions (e.g. deep plunge pool) and uncertainties involved.

Novak points out that

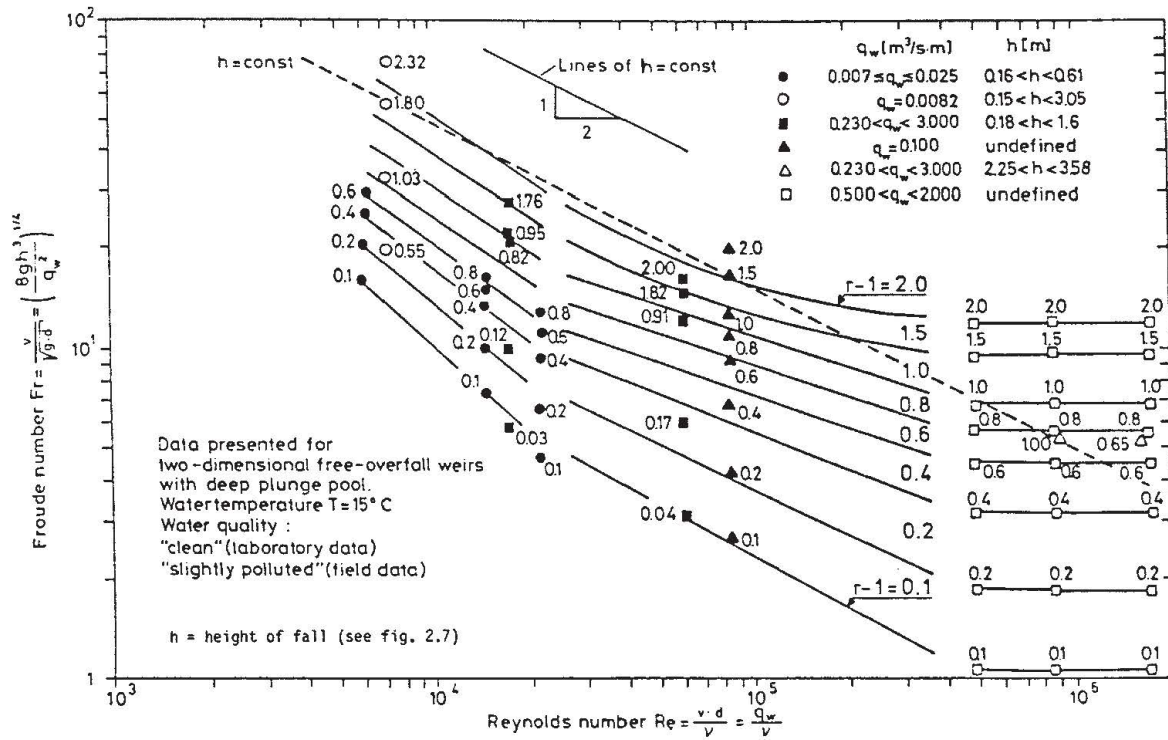- the plunge pool depth d_p affects the oxygen uptake markedly since it affects the bubble trajectories, and

Figure 2.8. Unified presentation of weir aeration data (rectangular weirs with deep plunge pools (Markofsky & Kobus, 1978)
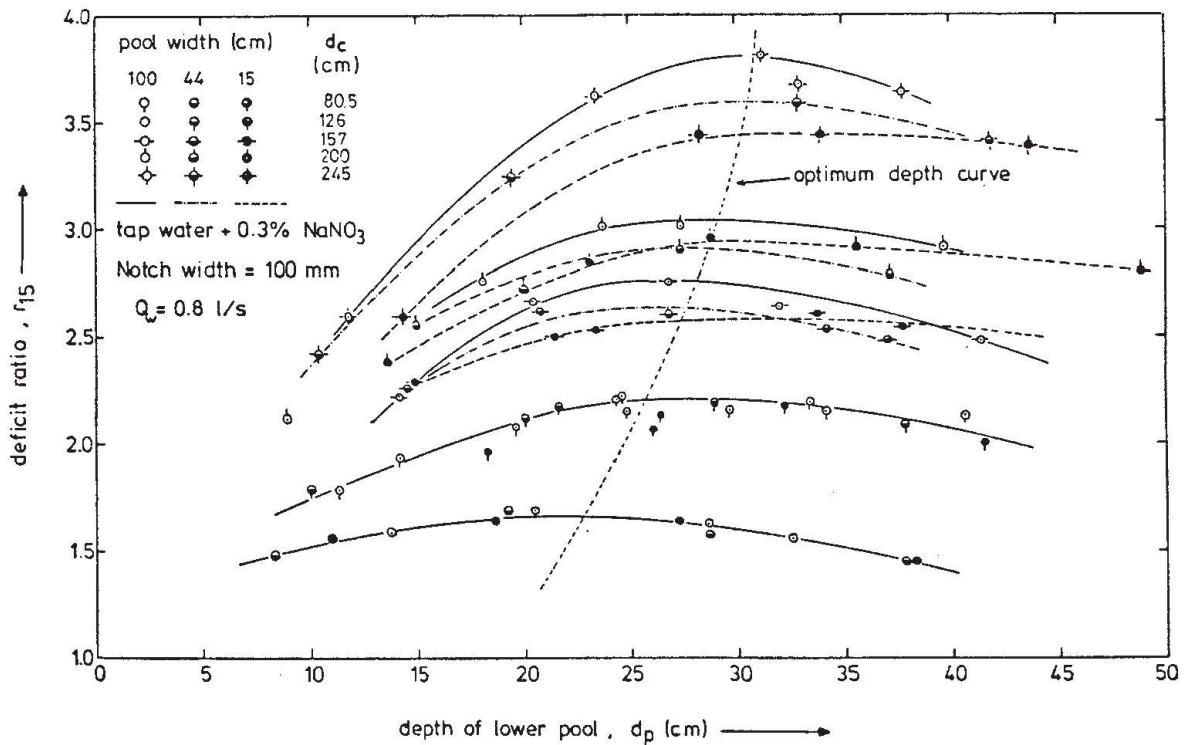

Figure 2.9. The influence of plunge pool depth on the reoxygenation rate at weir structures (Novak, 1980)

– that water quality and notably the salinity of the water have a significant effect on the mass transfer.

He gives an empirical correlation for the optimum depth d_p of the downstream pool, which corresponds roughly to the maximum penetration depth of the air bubbles. This correlation is given in dimensional form as

$$d_p \; |\mathrm{m}| = 0.00433 \, Re^{0.39} \cdot Fr_\mathrm{j}^{0.24} \tag{2.22}$$

At larger and at smaller plunge pool depths, the reoxygenation rate is less pronounced (Figure 2.9).

For this optimum depth, Novak gives the following equations for the reoxygenation rate r_{15} under standard conditions:

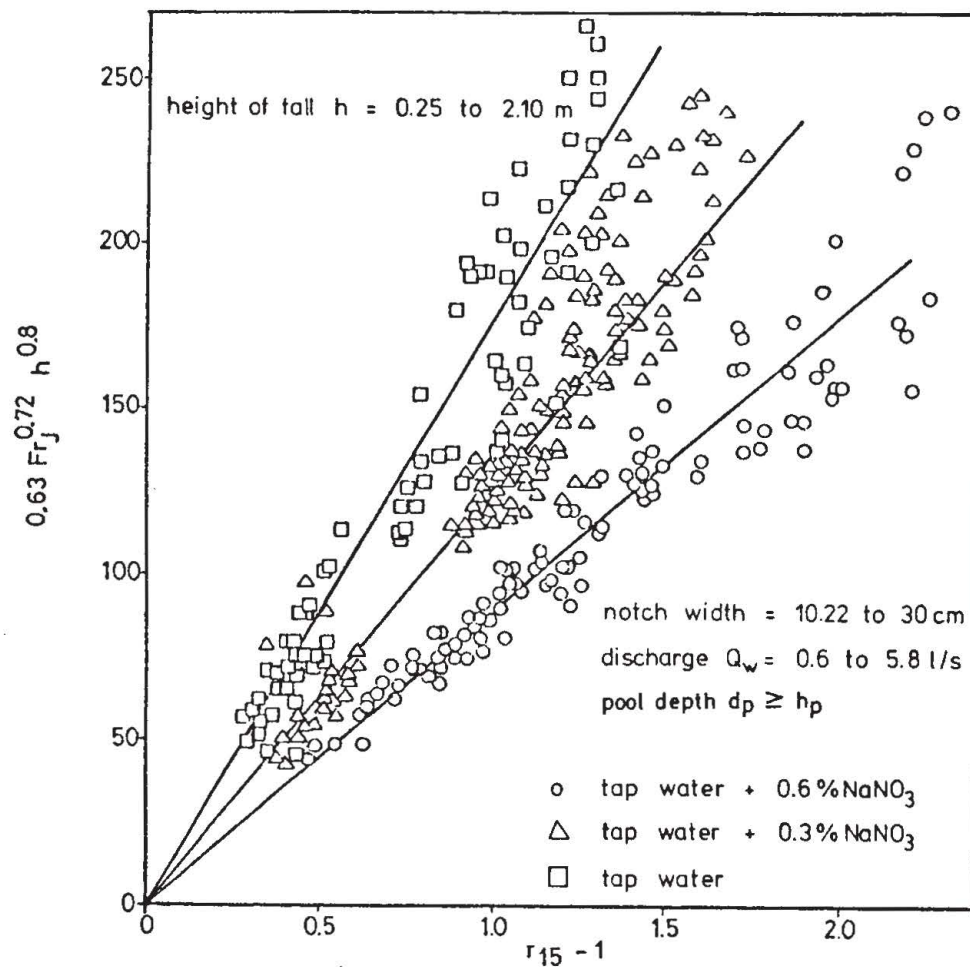$$r_{15}-1 = k_r \, Fr_j^{1.78} \cdot Re^{0.53} \tag{2.23}$$

Figure 2.10. Weir oxygenation: correlation of measurements with Equation 2.23 (Novak, 1980)

The coefficient k_r is given as a function of the salinity (sodium nitrite) in the following form

NaNO$_2$	k_r (–)
0 %	0.627 10^{-4}
0.3%	0.869 10^{-4}
0.6%	1.243 10^{-4}

A plot of Equation 2.23 with available data over a wide range of discharges and heads as given in Figure 2.10 shows consistent results.

2.6 HYDRAULIC JUMP

Air entrainment in rectangular hydraulic jumps in open channels has been studied by Rajaratnam (1962), Resch & Leutheusser (1972) and Schröder (1963). Figure 2.11 summarizes the experimental results.

Rajaratnam gives the relationship

$$\beta_e = q_{ae}/q_w = 0.018(Fr-1)^{1.245} \qquad (Fr \text{ from } 2.5 \text{ to } 9) \qquad (2.24)$$

However, the justification of the exponent chosen seems to be questionable in view of the experimental data (Figure 2.11). Renner gives the equation
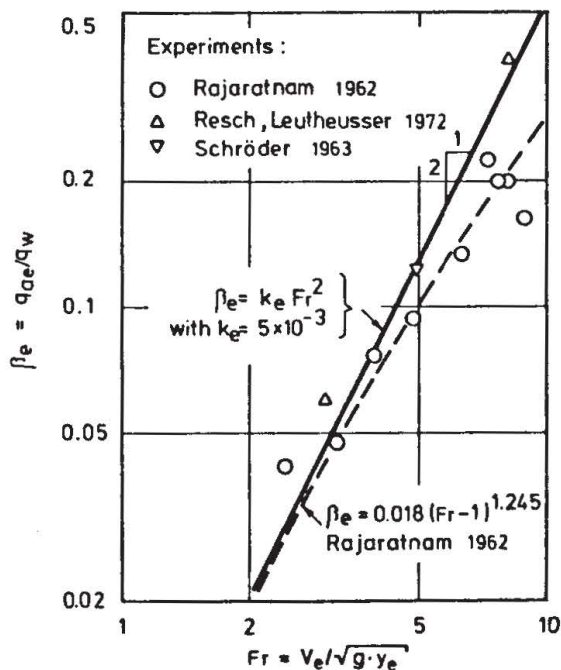

Figure 2.11. Air entrainment in a hydraulic jump

$$\beta_e = q_{ae}/q_w = 5 \times 10^{-3}\, Fr^2 \qquad (Fr \text{ from } 2.5 \text{ to } 9) \qquad (2.25)$$

As can be seen from Figure 2.11, both relationships give appropriate estimates for the entrainment at the toe of the hydraulic jump in the quoted range of Froude numbers. The spread of the data points in Figure 2.11 as well as a comparison of the two formulas for a given flow configuration give an indication of the degree of uncertainty in the estimate of q_{ae}.

Information on the bubble sizes and on air concentrations in the flow has been given by Leutheusser & Resch (1973). Figure 2.12 shows some experimental results which may be used as a guideline for corresponding estimates.

Mass transfer and oxygenation in hydraulic jumps have been investigated by Resch & Leutheusser (1974) and Novak et al. (1980). Novak has proposed the following correlation (see Figure 2.13) for the reoxygenation rate r_{15} under standard conditions at specific discharges experimentally verified in the range of 0.0146 to 0.0808 m²/s:

$$r_{15} - 1 = k_1\,(\Delta E/y_e)^{0.8}(q_w/q_o)^{0.75} \qquad (2.26)$$

with: ΔE = energy head loss due to hydraulic jump, $q_o = 0.0345$ m²/s (reference discharge), y_e = inflow water depth upstream of the hydraulic jump, and
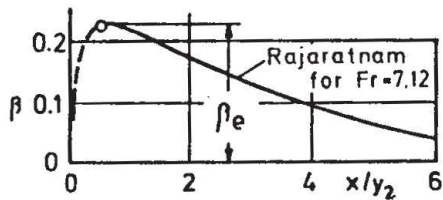
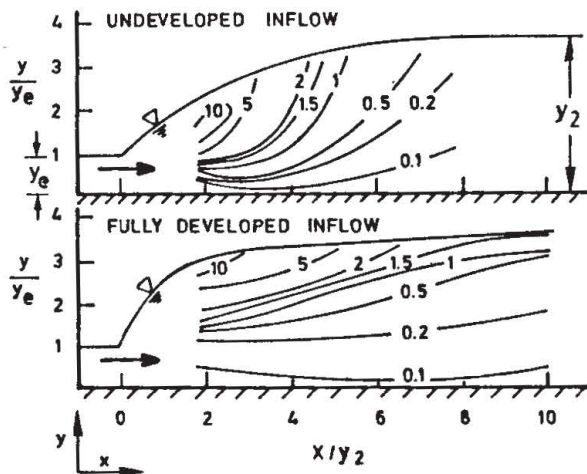Void ratio distribution [%] for
Fr = 2,85 according to Leutheusser (1973)

Figure 2.12. Detrainment in a hydraulic jump

NaNO$_2$	k$_1$ (–)
0 %	0.0158
0.3%	0.0186
0.6%	0.0230

Numerous studies have investigated hydraulic jumps in closed conduits at the transition from free-surface to pressurized flow. These studies cannot be compared directly to the free surface flow, because they may be strongly affected by the transport capacity of the pipe flow. This means that the measured entrainment rates reflect only the net transport capacity of the downstream conduit, which controls the process, and do not include the amount of air which is locally detrained (difference between q_{ae} and q_{at}). Hydraulic jumps in closed conduits are treated in monograph *Air-water flow in closed conduits*.
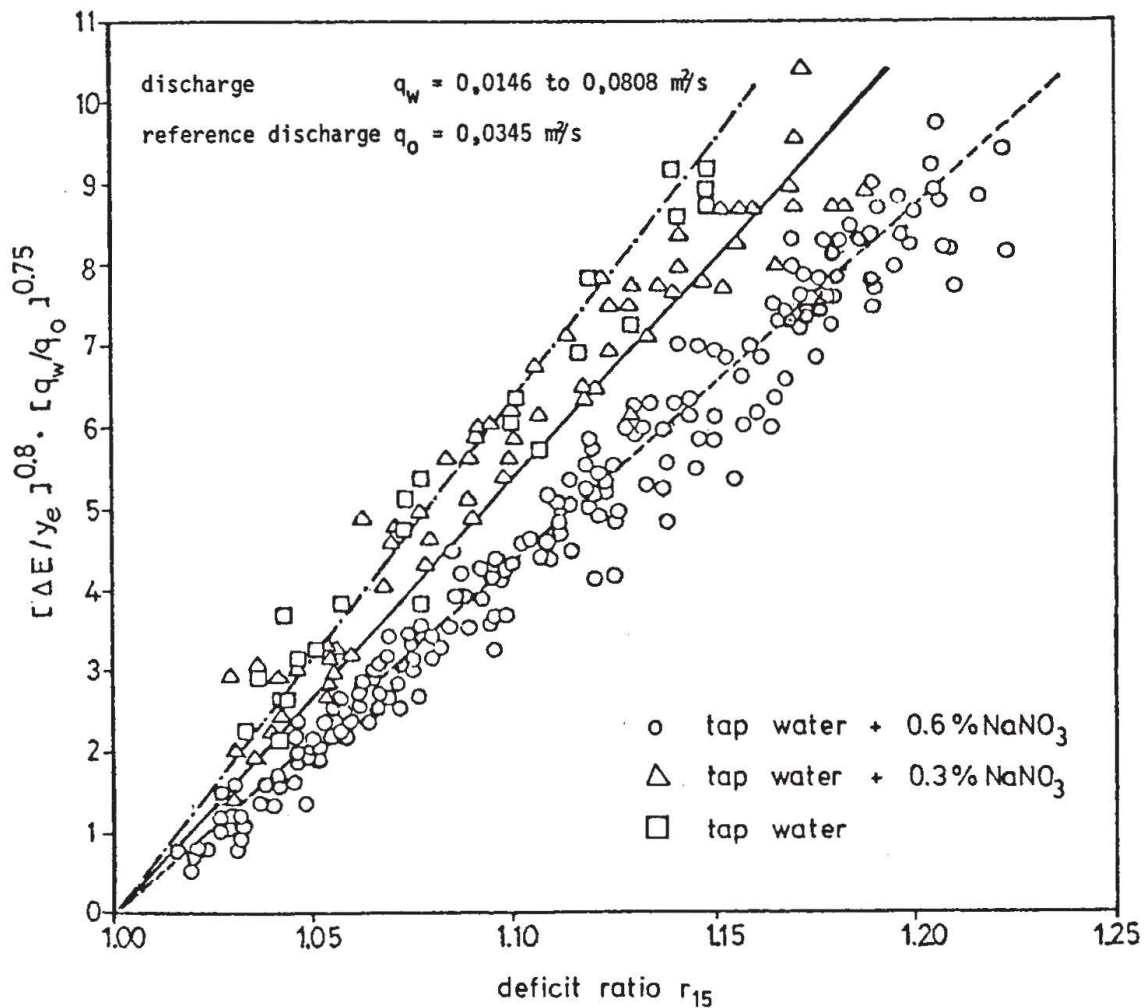

Figure 2.13. Oxygenation in hydraulic jumps: correlation of measurements with Equation 2.26 (Novak, 1980)

2.7 SIMILARITY CONSIDERATIONS FOR HYDRAULIC MODELS

2.7.1 *Modelling free surface flow with air entrainment*

Studies of local air entrainment and detrainment involve mostly experimental investigations on small scale models. Obviously, perfect dynamic similarity cannot be achieved; the modelling parameters as derived from dimensional analysis cannot be satisfied simultaneously in a small scale model using the same fluids, i.e. air and water. It is often argued that the bubble sizes generated by free-surface aeration always exhibit about the same absolute size and hence violate in a small scale model both geometric similarity (ratio bubble size to boundary scale) and dynamic similarity (ratio of bubble rising velocity to water velocity).

Complete similarity requirements are described by Equation 1.4. Restricting considerations to a small scale model which is geometrically similar, water of the same quality as in the prototype (i.e. Z = const) and entrainment from the atmosphere (i.e. c_{pe} = 0), this equation reduces to

$$\beta_e = f(Fr; Re; (Tu)) \tag{2.27}$$

If according to the model law for free surface flows the Froude number is kept the same in model and prototype by proper choice of the model velocity scale, then the *scale effects* are embedded in the fact that the Reynolds number is not modelled correctly, and hence neither are the turbulence characteristics (turbulence intensity, turbulent energy spectrum) of the flow. The parameter Tu stands for the turbulence characteristics of the approach flow in the inlet section of the model. Quite generally, since the model Reynolds number is always smaller than the corresponding value of the prototype, the effects of viscosity are exaggerated in the small scale model.

However, in fully turbulent flow the mean flow characteristics and the turbulence macroscale structure become independent of the Reynolds number, since the energy transfer in turbulence production from mean flow to macroscale turbulent eddies is dominated by inertial effects and viscosity becomes apparent only in the small scale dissipation of turbulent energy. Under such conditions, the resulting scaling requirement is reduced to the requirement that in either case the Reynolds number must be large enough so that fully turbulent flow conditions prevail. In prototype, this condition is usually met, and therefore this requires simply

$$Re_{model} \geq Re_t \tag{2.28}$$

where Re_t marks the minimum Reynolds number for fully turbulent flow. If the local values of water velocity and depth or thickness at the entrainment location

are used, then it is surmised that the value of Re_t is of the order of 10^5. However, no definite information about this value is available, and this limit may of course be different for different flow configurations. For instance, observations in plunging jets by Ervine (1985), indicate that there may still be an influence of the Reynolds number at values well beyond the estimate given above.

In hydraulic models, the approach flow conditions at the inlet section of the model have to be prescribed. Not only the mean flow properties, but also the turbulence properties of the approach flow (as characterized by the parameter Tu) may have a very significant effect upon the air entrainment processes. This fact is well demonstrated in Figure 2.4 and has also been shown in other investigations, in which the turbulence characteristics of the approach flow affected the entrainment characteristics as much as one order of magnitude. Thus, for proper hydraulic modelling, reproduction of the approach flow conditions must include proper reproduction of the turbulence characteristics (Tu).

The scaling relationship Equation 2.27 can be plotted, for given approach flow turbulence Tu, in general form as a graph of lines of constant β_e in a Fr-Re plane. Such a diagram is sketched in Figure 2.14. This diagram is the result of general
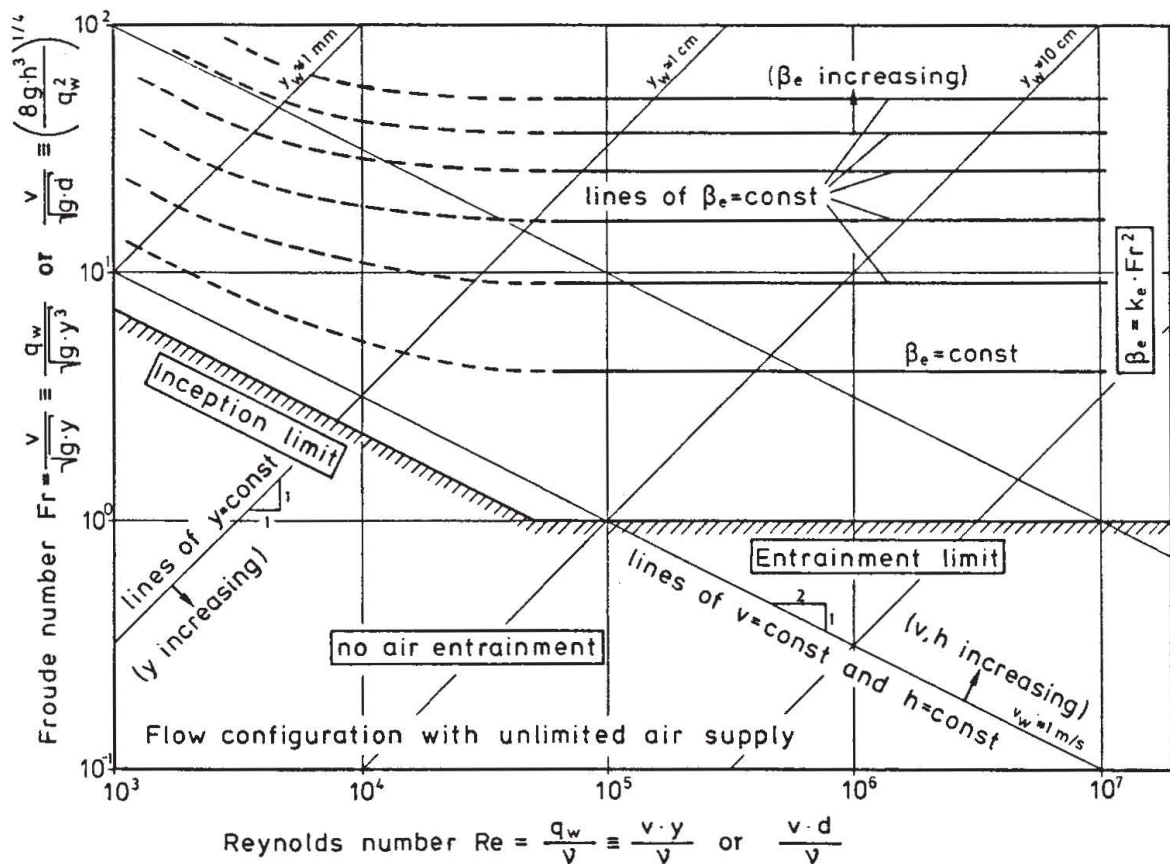

Figure 2.14. Suggested functional relationship for the relative air entrainment (for given approach flow turbulence)

similarity considerations and still requires verification by suitable experimental data. Since *Fr* and *Re* are both based on the same reference quantities, lines of constant velocity and of constant reference lengths can be identified in this plane.

Information about the form of the relationship can be obtained from consideration of the asymptotic behaviour at the inception limit and the entrainment limit under fully turbulent conditions.

For *plunging-jet configurations* like weirs, drop structures and siphons, the inception limit is important. Relationships of the form

$$q_{ae} = k\,(v - v_c)^3 \tag{2.29}$$

can be shown (see Thomas, 1984) to imply

$$q_{ae}/q_w = k\,Fr^2\,(1 - v_c/v)^3 \tag{2.30}$$

In contrast for *hydraulic-jump configurations* the entrainment limit is predominant. The relations of the general form

$$\beta_e = k_e\,(Fr - 1)^\alpha \tag{2.31}$$

approach in the limit the function

$$\beta_e = k_e\,Fr^2 \tag{2.32}$$

The conditions of fully turbulent flow are reached if the local Reynolds number exceeds the value Re_t as defined in Equation 2.28. For Froude models, the following relationship for the boundary length scale l_e at the location of entrainment has been derived (Kobus, 1984):

$$l_e \ge \left[\frac{Re_t}{Fr}\left(\frac{\mu_w/\rho_w}{\sqrt{g}}\right)\right]^{2/3} \tag{2.33}$$

For a given configuration, Equation 2.33 allows an estimate of the model dimensions required for fully turbulent flow. As an example, models of hydraulic jumps with $(Fr > 1)$ should satisfy Equation 2.33 for the lower limit $(Fr = 1)$ and hence necessarily also for all higher Froude numbers. This requires minimum water depths for critical flow of 10 cm for $(Re_t = 10^5)$ and 2 cm for $(Re_t = 10^4)$.

2.7.2 *Additional criteria for similarity of air transport and escape*

The question of transport and detrainment of air is closely linked to the question of the resulting bubble sizes. Since the bubble size distribution depends upon the turbulence characteristics of the flow (and hence on the Reynolds number),

transport and detrainment can also be expected to be Reynolds number dependent. The argument that bubble sizes in models are proportionally too large would hint at scale effects in the sense that detrainment is too large in the model and hence transport too small. This argument ties in with the fact that due to the lower turbulence level (smaller Reynolds number) the transport capacity in the model is expected to be smaller than in the prototype.

2.7.3 *Additional conditions for similarity of oxygen transfer*

Modelling mass transfer processes is even more uncertain due to the additional influence of the water quality. A discussion of Figure 2.8 illustrates well the scaling considerations for plunging jets. In the laboratory, for low flow rates and low heights of fall (lower left corner), surface tension prevents air entrainment and therefore reoxygenation from occurring. The effect of surface tension is overcome as a result of an increase in the flow rate or height of fall or both. Air is entrained to greater depths and, with increasing turbulence, is broken into finer and finer bubbles. Both effects increase the rate of gas transfer. Thus, reoxygenation increases with both q_w and h.

In the fully turbulent field situation, the amount of air entrainment is determined by the impingement velocity v_e at the nappe which is a function of the height of fall h only. Thus, the same quantity of air will be entrained for the same height of fall regardless of the flow rate. Therefore, with increasing water flow rate, less air per unit volume of water is available and thus the reoxygenation rate decreases. In the logarithmic parameter presentation, lines of constant h are given by straight lines with slopes of $(-1/2)$, i.e. parallel to the dashed line. Proceeding along such a line towards higher flow rates, i.e. to the right, one observes that for a constant height of fall, r decreases with increasing water discharge in the large-scale field situation. In contrast, r increases with increasing height of fall at a given water flow rate (vertical line).

Considering Froude models in Figure 2.8, one proceeds along a horizontal line (Fr = constant) from left to right (to large Re) in going from a small scale Froude model to the prototype situation. It is seen that the reoxygenation rate r will necessarily be smaller in the model than in the prototype. Laboratory experiments for the determination of reoxygenation rates r have therefore often been performed at prototype dimensions of h. Historically, the results of such studies have been presented in equations in which r is a function of h only (see references in Markofsky & Kobus, 1978) without consideration of the flow rate q_w. Such equations will plot as straight lines with a slope of $(-1/2)$, i.e. parallel to the dashed line in Figure 2.8. In these cases predictions of r from laboratory studies at low flow rates lead to overestimations of r for high flow rates at the same height of fall.

For any model study involving air entrainment, extreme care has to be taken that all parts of the flow configuration are modelled correctly, including the air

supply system. Thomas (1982) and others have demonstrated that even small changes in the geometry may greatly affect the air entrainment processes. For many problems, Froude models are adequate as long as the minimum model size as given by Equation 2.33 is maintained.

LIST OF SYMBOLS

b,B	|m|	width
c_{pe}	|-|	pressure coefficient $c_{pe} = \Delta p_e/(\rho_w v_w^2/2)$
D,d	|m|	diameter
d_n	|m|	nozzle diameter
d_p	|m|	plunge pool depth
d_c	|m|	distance weir crest to pool bottom
ΔE	|m|	energy head loss due to hydraulic jump
Fr	|-|	Froude number $Fr = v/\sqrt{gl_w}$
Fr_j	|-|	jet Froude number
g	|m/s^2|	gravitational acceleration
H	|m|	weir head
h	|m|	height of fall
h_p	|m|	penetration depth
k_r,k_1	|-|	coefficients
k_e	|-|	entrainment coefficient
l_e	|-|	boundary length scale
l_p	|m|	perimeter of a jet at the point of impact
l_w	|m|	reference length
l_t	|-|	turbulence length scale
L_o	|m|	jet break-up length
Q_{ae}	|m^3/s|	total rate of entrained air
q_{ae}	|m^2/s|	specific rate of entrained air per unit width
q_{at}	|m^2/s|	specific air transport rate per unit width
q_j	|m^2/s|	jet discharge per unit jet perimeter
q_t	|m^2/s|	net air transport
Q_w	|m^3/s|	water discharge
q_w	|m^2/s|	specific water discharge per unit width
r	|%|	reoxygenation rate
r_{15}	|%|	reoxygenation rate under standard conditions
R	|m|	hydraulic radius of the jet at impact
Re	|-|	Reynolds number $Re = v_w \cdot l_w/(\mu_w/g)$
Re_t	|-|	minimum Reynolds number for fully turbulent flow
Tu	|-|	turbulence characteristics
v	|m/s|	velocity
v_c	|m/s|	critical velocity

v_e |m/s| velocity at the line of air entrainment, impingement velocity

v_n |m/s| velocity at nozzle

v_t |m/s| turbulent fluctuations (RMS)

v' |m/s| velocity fluctuations

v_w |m/s| water velocity

We |–| Weber number $We = v_w / \sqrt{(\sigma_{wa} / \rho_w . l_w)}$

y |m| water depth

y_2 |m| outflow water depth downstream of the hydraulic jump

y_e |m| water depth at the point of air entrainment, inflow water depth upstream of the hydraulic jump

Z |–| liquid parameter $Z = g\, \mu_w^4 / \rho_w \sigma_{wa}^3$

β_e |–| relative air entrainment $\beta_e = q_{ae} / q_w$

ρ_w |kg/m³| density of the liquid (water)

μ_w |kg/ms| dynamic viscosity of the liquid (water)

ν_w |m²/s| kinematic viscosity of the liquid (water)

σ_{wa} |N/m| surface tension at the gas-liquid (air-water) interface